Preferential Binding of Equine Ferricytochrome *c* to the Bacterial Photosynthetic Reaction Center from *Rhodobacter sphaeroides*†

Jonathan W. Larson‡ and Colin A. Wraight*,‡

Department of Biochemistry and Center for Biophysics and Computational Biology, University of Illinois at Urbana−Champaign, Urbana, Illinois 61801

Received June 6, 2000; Revised Manuscript Received September 26, 2000

ABSTRACT: Redox titration of horse heart cytochrome *c* (cyt *c*), in the presence of varying concentrations of detergent-solubilized photosynthetic reaction center (RC) from *Rhodobacter sphaeroides*, revealed an RC concentration-dependent decrease in the measured cyt *c* midpoint potential that is indicative of a 3.6 ± 0.2-fold stronger binding affinity of oxidized cytochrome to a single binding site. This effect was correlated with preferential binding in the functional complex by redox titration of the fraction of RCs exhibiting microsecond, first-order, special pair reduction by cytochrome. A binding affinity ratio of 3.1 ± 0.4 was determined by this second technique, confirming the result. Redox titration of flash-induced intracomplex electron transfer also showed the association in the electron transfer-active complex to be strong, with a dissociation constant of 0.17 ± 0.03 μM. The tight binding is associated with a slow off-rate which, in the case of the oxidized form, can influence the kinetics of P^+ reduction. The pitfalls of the common use of xenon flashlamps to photoexcite fast electron-transfer reactions are discussed with relation to the first electron transfer from primary to secondary RC quinone acceptors. The results shed some light on the diversity of kinetic behavior reported for the cytochrome to RC electron-transfer reaction.

The bacterial photosynthetic reaction center (RC)[1] from *Rhodobacter sphaeroides* is a three subunit integral membrane protein that catalyzes light-induced reduction of ubiquinone to ubiquinol using soluble cytochrome c_2 (cyt c_2) as electron donor. Following flash activation, rapid electron-transfer events produce a charge separation between the primary electron donor, P, a dimer of bacteriochlorophyll, and the primary quinone, Q_A (*1*). Subsequently, the electron is transferred to the secondary quinone, Q_B, and the photooxidized P (P^+) is re-reduced by cyt c_2 (*2*). In isolated RCs, P^+ can be reduced by a variety of *c*-type cytochromes before back reaction from the quinone acceptors occurs (*3*). The cytochrome to P^+ electron transfer reaction has been extensively studied, and a bewildering array of kinetic behaviors has been described (reviewed in refs *4* and *5*). So far no clear rationalization of the differences has been presented. In this work, we describe a likely source of some of the discrepancies in the literature.

Electrostatic interactions stabilize RC−cytochrome association (*6*−*8*). Although the RC transmembrane-spanning domain has overall 2-fold rotational symmetry, there is an asymmetric patch of negative electrostatic potential on the M-subunit side of the RC periplasmic surface, arising from a cluster of acidic residues (*9*, *10*). This region interacts favorably with the positive electrostatic potential surrounding the solvent-exposed heme edge of the cytochrome due to a cluster of lysine residues (*11*−*16*). This mode of interaction is quite general for the association of *c*-type cytochromes with their different physiological partners, and the cluster of lysine residues surrounding the heme cleft is highly conserved (*17*).

Cocrystallization of RCs with the native cyt c_2 shows some electron density indicative of asymmetric binding to the M-subunit side, above the center of negative electrostatic potential (*18*). X-ray crystal structures have been determined both for RCs and for several *c*-type cytochromes separately (for RCs, see refs *19*−*23*; for horse heart cytochrome *c* (cyt *c*), see ref *24*; for cyt c_2, see ref *25*). Calculations of binding enthalpies yield an energy minimum for the asymmetric configuration (*10*, *18*), but the population of RC−cytochrome complexes may be an ensemble of isoenergetic rotational and/or translational orientations about that center (*3*). Different orientations and distances between redox centers may explain the polyphasic behavior of rapid, intracomplex electron transfer (*3*, *11*, *26*).

Two types of kinetic behavior have been reported for cytochrome oxidation. In the simple case (type I), the kinetics are consistent with cytochrome binding to a single, rapid electron transfer-active site. Intracomplex electron transfer produces a cytochrome concentration-independent fast phase. At subsaturating concentrations for complex formation, a rate-limiting second-order collisional interaction, followed by rapid first-order electron transfer, produces a slower,

† Work supported by the National Science Foundation (NSF MCB99-05672). J.W.L. was supported in part by a DOE/NSF/USDA Triagency training grant (DE-F902-92ER20095).

* Address correspondence to this author (cwraight@uiuc.edu).

‡ Present address: 600 S. Mathews Ave., Urbana, IL 61801.

[1] Abbreviations: RC, reaction center; cyt c_2, *Rhodobacter sphaeroides* cytochrome c_2; P, primary donor; Q_A, primary quinone acceptor; Q_B, secondary quinone acceptor; P^+, oxidized primary donor; cyt *c*, horse heart cytochrome *c*; LDAO, lauryldimethylamine oxide; TMPD, *N*,*N*,*N*′,*N*′-tetramethyl-*p*-phenylenediamine dihydrochloride; Fe-EDTA, ferric monosodium ethylenediaminetetraacetic acid; Q_6, ubiquinone-6; PC RCs, RCs reconstituted into phosphatidylcholine vesicles; LDAO RCs, LDAO solubilized RCs.

10.1021/bi0012991 CCC: $19.00
Published on Web 11/10/2000

cytochrome concentration-dependent phase. Simple kinetics have been reported many times with the native cyt c_2 (*3*, *27*−*29*), but only once with cyt *c* (*27*).

In other cases (type II), biphasic cytochrome oxidation kinetics comprise a cytochrome concentration-independent fast phase that matches the fast-phase lifetime of the simple kinetic case and a concentration-dependent slow phase that accelerates with increasing cytochrome concentration to a saturated pseudo-first-order rate that is slower than the fast phase. More generally, the fast phase, indicative of cytochrome bound in an active configuration before the flash, may consist of two components (*3*, *14*, *26*). The distinguishing feature of type II kinetics is that the total fast-phase amplitude does not account for all the kinetics at high cytochrome concentration but saturates at a value less than 1. Type II kinetics have been observed with both cyt *c* (*3*, *26*, *30*, *31*) and cyt c_2 from *R. sphaeroides* (*3*, *11*, *30*, *32*, *33*). They are described by a model in which cytochrome binds either in an electron transfer-active *proximal* configuration or in a mutually exclusive electron transfer-inactive *distal* configuration (*32*, *34*). Distally oriented cytochrome must first move to the proximal state in a first-order process before electron transfer can occur. Results from viscosity dependence studies are consistent with this transition having a physical mechanism of cytochrome rotation and/or translation across the RC periplasmic surface (*30*). Type II kinetics with cyt c_2 have been correlated with the RC tendency to aggregate (*35*), but no cause for this effect has been identified in either protein isolation techniques or methods of kinetic observation.

In this work, the effect of cytochrome redox state on binding affinity to the RC is studied by equilibrium and flash-induced kinetic redox titration techniques. It is concluded that oxidized cytochrome binds preferentially to detergent-solubilized RCs, as expected from a simple increase in Coulombic attraction between a more positively charged oxidized cytochrome and the RC. Oxidized cyt *c* also binds preferentially to purified mitochondrial bc_1 ubiquinol−cytochrome oxidoreductase (*36*), to purified cytochrome oxidase and succinate−cytochrome *c* reductase (*37*), and to purified RCs reconstituted into neutral phosphatidylcholine vesicles (*30*). Multiple binding sites were implicated in the latter case, with uncertain relation to electron transfer. Kinetic studies were performed here to correlate redox state-sensitive binding with the electron transfer-active complex.

EXPERIMENTAL PROCEDURES

Materials. Reaction centers were purified from *R. sphaeroides*, strain R-26, according to ref *38*. Following final purification to $A_{280\,nm}/A_{802\,nm} < 1.3$ (*39*), they were dialyzed against 0.03% lauryldimethylamine oxide (LDAO) and 10 mM Tris (pH 8.0), concentrated to 100 μM using a pressure cell with an Amicon XM-50 filter, and stored at −80 °C. The RC concentration was determined by absorbance measurement at 802 nm ($\epsilon_{802\,nm} = 288\ mM^{-1}\ cm^{-1}$, from ref *40*) on a diode-array spectrophotometer (Hewlett-Packard, 8452A).

Cyt *c* (Sigma Type VI) was reduced by sodium ascorbate, purified on a CM Sepharose cation-exchange column, and dialyzed against deionized water. The cytochrome was washed on the column with 50 mM NaCl and eluted at 300 mM following (*30*). The stock concentration was determined by absorbance measurement at 550 nm ($\epsilon_{550\,nm} = 27.6\ mM^{-1}\ cm^{-1}$, from ref *41*) on the diode-array spectrophotometer.

All optical samples contained 10 μM cyt *c*, 2 mM KCl, 10 mM Tricine (pH 8.0), 0.045% LDAO, 10 μM *N*,*N*,*N*′,*N*′-tetramethyl-*p*-phenylenediamine dihydrochloride (TMPD), and 10 μM Fe-EDTA. When used, ubiquinol-6 (Q_6) from ethanol was added to detergent solution (0.045% LDAO) followed by brief heating in a boiling water bath until the sample turned optically clear. After being cooled to room temperature, salt and pH buffer were added, followed by RCs and cytochrome. Redox potential measurements were performed in an anaerobic glass cuvette, and samples were purged for 0.5 h by blowing argon across the sample surface while stirring. Redox mediators were added after purging, and small aliquots of sodium ascorbate added to achieve reducing conditions before oxidative titration.

Redox Potentiometry. Redox potentiometry was performed using a handmade Ag|AgCl reference electrode potted in a 1 M KCl/2.5% agarose gel inside a Pasteur pipet. A total of 2 mM KCl was added to all optical samples to minimize the effect of salt leaching from the electrode. Conductivity measurements using a Yellow Springs Instruments 3403 electrode confirmed that the KCl concentration did not increase by more than 0.5 mM over a typical 1-h titration. In combination with the 10 mM pH buffer used, the effect of salt leaching on conductivity was less than 15%. Each sample was successively titrated in oxidizing (potassium ferricyanide added) and reducing (sodium ascorbate added) directions to confirm equilibrium and to verify that the changes in salt concentration do not significantly affect redox behavior.

The redox electrode was calibrated each day against the potassium ferri/ferrocyanide redox couple according to ref *42*. Redox potential changes were monitored continuously by a 12-bit analog-to-digital converter (Computer Boards, CIO-DAS08/Jr-AO), buffered by a Burr Brown OPA227PA set up as a 10× noninverting amplifier. Redox mediator concentration was high enough to ensure rapid electrode response times (usually within 10 s), but no mediator interference in micro or millisecond electron-transfer kinetics was observed.

Spectrophotometry. Ground-state and kinetic absorbance changes were monitored with a spectrophotometer of local design. Large area silicon (Hamamatsu, S3950-01) and InGaAs (Fermionics, FD3000W) photodiodes with locally designed current-to-voltage preamplifiers (10-μs response times) were used for light measurement in the visible and infrared, respectively. For cyt *c* redox measurement, monochromatic light from a 55-W quartz tungsten halogen bulb was selected by an ISA Triax-180 monochromator (3 mm fwhm) before passing through the sample into the detector. Detector output was monitored simultaneously with redox potential on a different channel of the same analog-to-digital converter as above.

P^+ reduction kinetics were measured at 1250 nm. The actinic component of the measuring beam was removed by a 1000 nm long pass edge filter (Andover, 100FH90-25) before passing through the sample. After the sample, the same monochromator as above was used to select the measuring wavelength (1250 nm, 14 nm fwhm) and to remove the actinic flash. Automated, DC-coupled baseline subtraction and active RC-filtering of the detector output was

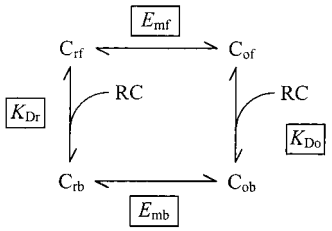

FIGURE 1: Equilibrium model of redox state-sensitive RC−cytochrome binding, including reduced free (c_{rf}), oxidized free (c_{of}), reduced bound (c_{rb}), and oxidized bound (c_{ob}) cytochrome; free RCs (RC); midpoint potentials for free (E_{mf}) and bound (E_{mb}) cytochrome; and dissociation constants for reduced (K_{Dr}) and oxidized (K_{Do}) cytochrome.

performed by a digitally programmable signal conditioning unit of local design before analog-to-digital conversion with a 12-bit, 1 MHz data acquisition card (Computer Boards, M1).

Unless specified, flash excitation was provided by a frequency doubled Nd:YAG laser pulse (532 nm) with a fwhm of < 10 ns (Continuum, Surelite I). The beam width was expanded before striking the sample to provide uniform saturating illumination. When mentioned, a red-filtered (3 mm RG-9 Schott glass) xenon flashlamp (EG&G, FX-200) with a 19-μs fwhm was also used. The flashlamp discharge profile was measured at 50 ns time resolution (Keithley, PCIP−Scope) with a 0.7 GHz frequency response, high-speed PIN photodiode (Advanced Photonix, Inc. SD 020-11-33-211).

Both cyt *c* and TMPD absorbances change with redox state at 532 nm, the wavelength of actinic emission. To verify constant flash saturation throughout redox titrations, an identical RC sample to those used in experiment was prepared in the anaerobic cuvette without cyt *c* and TMPD. A second cuvette containing reduced cytochrome and TMPD was placed between the RC sample and the actinic source. The amplitude of flash-induced P^+ formation was unaffected by oxidation of the cytochrome−TMPD sample.

Numerical Methods. Unless mentioned otherwise, data fit analysis was performed using a modified Levenberg−Marquardt algorithm (MicroCal Origin 5.0). Two redox titrations were performed for each condition. Individual fits (Levenberg−Marquardt or otherwise) were performed on each redox titration, and the fit parameters were reported as their average best-fit value, plus or minus the standard deviation.

Euler's method was used for numerical solution of differential equations. The error in the results was estimated by halving the number of points used (doubling the time between points, Δt), and the resultant values were less than 0.03% different from original calculation. The error using Euler's method is at most proportional to Δt (*43*); therefore, subsequent refinements to the solutions by increasing the time resolution or switching to a more sophisticated numerical approach will yield insignificant improvements.

Theoretical Model of Preferential Binding. If cytochrome binds preferentially in either of its redox states, the midpoint potential of bound cytochrome shifts according to

$$E_{mb} = E_{mf} + \frac{RT}{F}\ln\left(\frac{K_{Do}}{K_{Dr}}\right) \quad (1)$$

where E_{mb} and E_{mf} are the midpoint potentials of bound and free cytochrome and K_{Dr} and K_{Do} are the dissociation constants for reduced and oxidized cytochrome. However, in typical titrations the absorbance changes of bound and free forms cannot be distinguished. Consequently, determination of redox midpoint depression from experiments that measure the ratio of total reduced versus oxidized cytochrome requires complete solution of the binding model in Figure 1. This system is described by five independent equations:

$$c_{tot} = c_{rf} + c_{of} + c_{rb} + c_{ob}$$

$$[RC]_{tot} = [RC] + c_{rb} + c_{ob}$$

$$\frac{c_{rf}}{c_{of}} = e^{(E_{mf} - E_h)(F/RT)} = \alpha_f$$

$$\frac{c_{rb}}{c_{ob}} = e^{(E_{mb} - E_h)(F/RT)} = \alpha_b$$

$$K_{Dr} = \frac{[RC]c_{rf}}{c_{rb}}$$

where c_{rf}, c_{of}, c_{rb}, c_{ob}, and K_{Dr} are as defined in Figure 1, and where $[RC]_{tot}$ and c_{tot} are the total RC and cytochrome concentrations, respectively. Solution of this nonlinear system of equations is

$$c_{ob} = \frac{-b \pm \sqrt{b^2 - 4c}}{2}$$

$$c_{rb} = \alpha_b c_{ob}$$

$$c_{of} = \frac{c_{tot} - c_{ob}(1 + \alpha_b)}{1 + \alpha_f}$$

$$c_{rf} = \alpha_f c_{of}$$

$$[RC] = [RC]_{tot} - c_{rb} - c_{ob}$$

where

$$b = -\left(\frac{[RC]_{tot} + c_{tot}}{1 + \alpha_b} + \frac{K_{Dr}\alpha_b(1 + \alpha_f)}{\alpha_f(1 + \alpha_b)^2}\right)$$

and

$$c = \frac{c_{tot}[RC]_{tot}}{(1 + \alpha_b)^2}$$

Figure 2 shows theoretical titration curves (points) at constant total cytochrome but varying RC concentrations, using experimentally determined values for K_{Dr} (*3*, *26*, *30*) and E_{mf} (*30*) and assuming 5-fold preferential binding of the oxidized form ($K_{Do} = 5K_{Dr}$). The lines are best fits to the Nernst equation, and it is easy to see how preferential binding of oxidized cytochrome could be overlooked. The effective redox midpoint potential depression of a typical sample containing 10 μM cyt *c* and 2 μM RCs is only 9 mV, a difference often lost in the noise of redox titration of

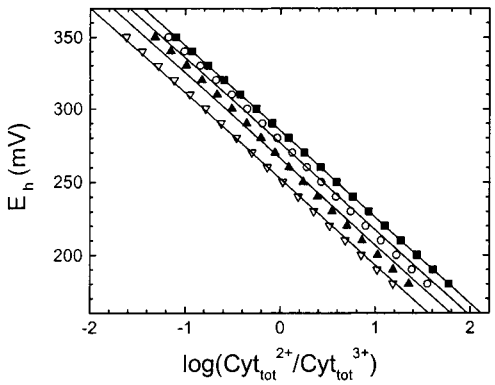

FIGURE 2: Solution of the equilibrium binding model in Figure 1 for E_{mf} = 280 mV, E_{mb} = 236 mV, K_{Dr} = 1 μM, c_{tot} = 10 μM, and RC_{tot} = 0 (squares), 2 (circles), 5 (up triangles), and 10 μM (down triangles). Lines are best fits to a single Nernst component.

biological samples. The predicted sigmoidicity, most apparent in Figure 2 at 2 and 5 μM RCs, is also too small for observation within typical experimental precision.

Redox potential change as a function of absorbance difference (A) was fit to the function

$$E_h(A) = E_m + \frac{RT}{F}\ln\left(\frac{A_r - A}{A - A_o}\right)$$

where A_r and A_o are fit parameters for the absorbance differences of fully reduced and fully oxidized cytochrome, respectively. This function is only intended as an empirical fit for the purpose of determining A_r and A_o in samples containing RCs, although χ^2 goodness-of-fit analysis showed that the model fits titrations with and without RCs equally well. For purpose of comparison to the theoretical model (e.g., Figure 4), the data are transformed to the fraction of total cytochrome reduced according to

$$\text{fraction reduced} = \frac{A - A_o}{A_r - A_o}$$

where A_r and A_o are determined from fit.

RESULTS

Ground-State Cytochrome Redox Titration. Reduced 10 μM cyt *c* was titrated with potassium ferricyanide and sodium ascorbate in the presence of 0, 2, and 5 μM RCs. Higher RC concentrations, such as equimolar RC−cyt c, were avoided to conserve material. Absorbance changes were monitored at the cyt *c* α-peak at 550 and 577 nm, and the difference was taken to remove the component due to TMPD redox-state changes. TMPD absorbance changes are the same at these two wavelengths (Figure 3).

Best-fit midpoint potentials for cyt *c* alone were 285 ± 2 and 280 ± 1 mV for the two experiments (uncertainties based on fit). The difference in values is likely due to variation in reference electrode calibration, but both values are in close agreement with previous reports (*30*, *44*). Since the difference in cyt *c* midpoint potential most likely reflects a systematic offset in all measurements, the results from the two experiments are superimposed in Figure 4A with the redox potentials from Figure 4C linearly offset such that the free cytochrome midpoint potentials match. It is clear from Figure 4A that cyt *c* titrates at successively lower redox potentials with increasing RC concentration.

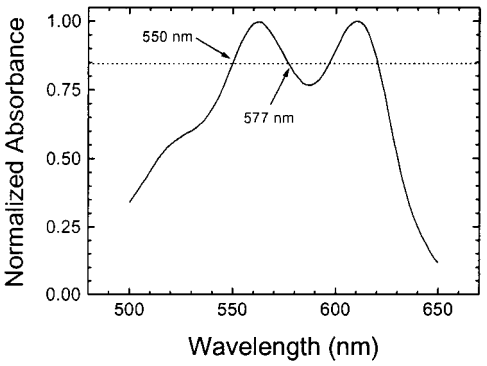

FIGURE 3: Redox difference spectrum of oxidized minus reduced TMPD. Conditions: (reducing) 12 μM TMPD reduced with small additions of sodium ascorbate and (oxidizing) the same concentration TMPD oxidized with small additions of potassium ferricyanide.

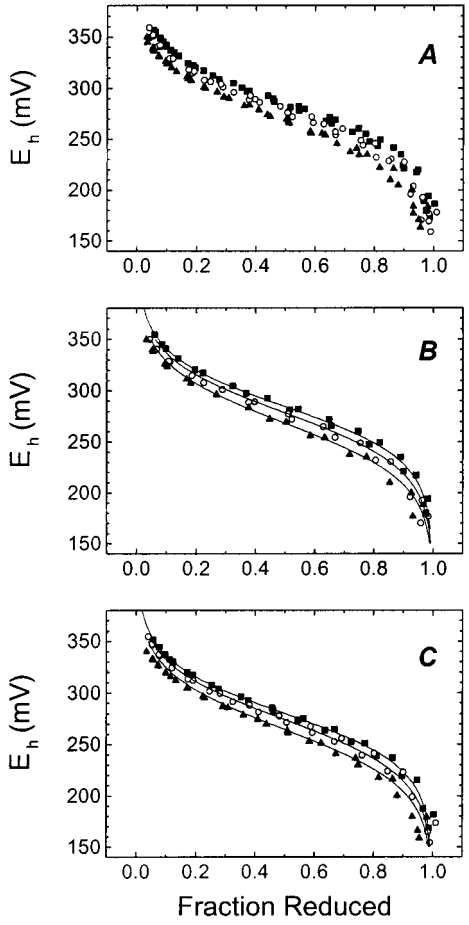

FIGURE 4: Cyt *c* redox titration at varying [RC]. (A) Superposition of two separate sets of titrations, as explained in text. (Squares) just cytochrome, (circles) plus 2.2 μM RCs, and (triangles) plus 5.5 μM RCs. (B and C) Individual sets of titrations from panel A, at varying [RC], compared to the redox state-sensitive binding model of Figure 1. Same symbols as in panel A. Fit parameters as follows: K_{Dr} = 0.17 μM; RC_{tot} = 0, 2.2, and 5.5 μM; c_{tot} = 10.1 μM; (B) E_{mf} = 284.6 mV, E_{mb} = 251.0 mV; and (C) E_{mf} = 280.1 mV, E_{mb} = 248.1 mV. Conditions: 10.1 μM cyt *c*, 10 mM Tricine (pH 8.0), 2 mM KCl, 0.045% LDAO, 10 μM TMPD, and 10 μM Fe-EDTA.

Figure 4B,C compares the changes in redox titration behavior to the theoretical model. Both titrations with 2 and 5 μM RCs were fitted simultaneously for the change in

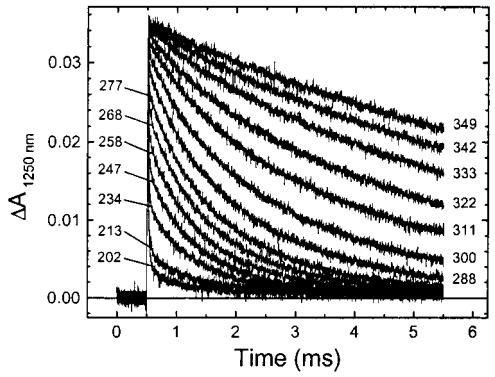

FIGURE 5: Redox titration of flash-induced P^+ reduction kinetics by cyt *c*. Redox potentials as indicated. Conditions as in Figure 4, with 2.2 μM RCs.

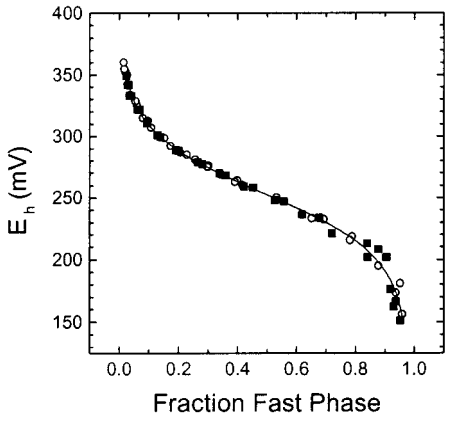

FIGURE 6: Redox titration of fast-phase amplitudes compared to redox state-sensitive binding model in Figure 1. (Squares) Taken from data in Figure 5, with the fraction fast phase determined as described in text. (Circles) Same conditions as squares, except RCs reconstituted with 10 μM Q_6, as described in Experimental Procedures. (Line) Model using the average best-fit values for the individual titrations: $E_{mf} = 282.35$ mV, $E_{mb} = 253.03$ mV, $K_{Dr} = 0.17$ μM, $RC_{tot} = 2.2$ μM, and $c_{tot} = 10.1$ μM.

midpoint potential of the bound cytochrome using χ^2 analysis weighted for the difference in number of data points per titration. The best-fit values for the midpoint potential depression in the individual experiments were 33.6 and 32.0 mV, using $K_{Dr} = 0.17$ μM (determined in next section).[2] The fits are shown in Figure 4B,C. Using eq 1, the result implies that oxidized cyt *c* binds 3.6 ± 0.2 times more tightly than the reduced form.

Redox Titration of P^+ Reduction Kinetics. Redox titration of flash induced cyt *c* oxidation was performed to correlate preferential binding of oxidized cyt *c* observed in the ground-state redox titrations with functional binding to the RC periplasmic surface. Figure 5 shows titration of P^+ reduction kinetics using identical experimental conditions as in the ground-state measurements. The relative amplitude of the fast phase indicates the equilibrium fraction of RCs that have bound reduced cyt *c*. Monitoring changes in the relative amplitude of this phase with change in redox potential provides a direct measure of the redox midpoint potential of functionally bound cytochrome.

Due to limited instrument response time, the fast phase is not completely resolved. Rather, its extent was inferred based on a missing amplitude technique. The first 140 μs after the flash was truncated to remove the fast phase, and the full amplitude of the slow phase was obtained by extrapolating back to the time of the flash, using empirical analysis (single-exponential extrapolation for low potentials and linear extrapolation for high potentials). The total P^+ amplitude was obtained by extrapolating the slow-phase amplitudes vs E_h to fully oxidizing conditions, using a fit to the Nernst equation. The resulting value was indistinguishable from the absorbance change at the same RC concentration without donor. The fast-phase fraction was then determined as

$$\text{fast-phase fraction} = 1 - \frac{\text{slow-phase amplitude}}{\text{total } P^+ \text{ amplitude}}$$

In general, for preferential binding, the midpoint potential of the bound complex cannot be determined by direct comparison of the fast-phase redox titration to the Nernst equation because the total concentration of bound cytochrome (oxidized plus reduced) changes throughout the titration. Although the form of the Nernst equation is maintained when the free ligand concentration is in great excess (*45*), this simplifying assumption is not valid here. Instead, a general solution was obtained by equating the fast-phase fraction with the concentration of bound, reduced cytochrome divided by the total RC concentration. The total bound cyt *c*/RC ratio was calculated as a function of E_h from analytical solution of the binding model in Figure 1.

Figure 6 compares redox titrations of the fast phase, both with and without RC reconstitution with exogenous quinone, to theoretical expectations based on best fitted values of 253.03 ± 0.04 mV and 0.17 ± 0.03 μM for E_{mb} and K_{Dr} ($= 1/K_{Ar}$), respectively.[3] This corresponds to a midpoint depression of 29 ± 3 mV for bound cyt *c* based on the average midpoint potential of free cyt *c* ($E_{mb} = 282 \pm 3$ mV) determined in the equilibrium studies. Equivalently, this implies 3.1 ± 0.4-fold preferential binding of the oxidized form. Systematic errors, e.g., in RC and cyt c stock concentrations, are not included in the estimate of K_{Dr} but are less than 10%.

A fraction of the RC population loses the secondary quinone acceptor during isolation. Those RCs containing only the primary quinone acceptor will be photochemically inactive if the semiquinone photoproduct from previous excitation is not oxidized by the mediator pool during dark adaptation (~1 min). On the other hand, RCs reconstituted with excess quinone can undergo multiple turnovers with less than 10% difference in quantum yield of charge separation for RCs with oxidized and reduced acceptor sides. It is clear from Figure 6 that no difference appears between the two sample types, confirming that sufficient dark adaptation was allowed for acceptor side oxidation with or without exogenous quinone.

Xenon Flashlamp vs Nd:YAG as Actinic Source. Xenon flashlamps are commonly used for actinic illumination, but their relatively long profile urges caution in their use for photoexciting fast electron-transfer reactions such as cyto-

[2] Best-fit values were determined by scanning E_{mb} from 230 to 300 mV with a 0.1-mV step size.

[3] The χ^2 best-fit values were determined by a grid search of E_{mb} and K_{Ar} parameter space with 0.05 mV and 0.2×10^6 M^{-1} resolution, respectively.

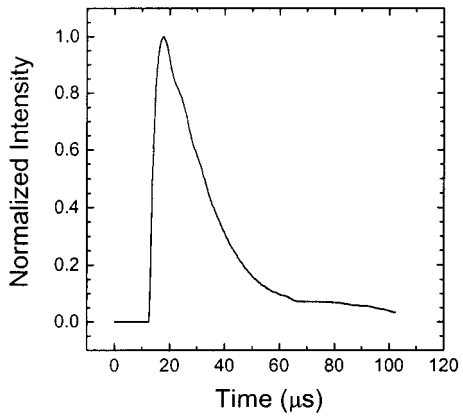

FIGURE 7: Xenon flashlamp discharge profile (EG&G, FX-200). 1.2 kV discharge voltage at 13 μF capacitance.

chrome oxidation by the RC. When measured through a RG-9 red filter, the full-width at half-maximum discharge is 19 μs for the EG&G FX-200 xenon flashlamp used here (Figure 7).[4] This is comparable to, or exceeds, the half-time of rapid, first-order electron transfer from cytochrome to P^+ (15−30 μs, from refs *3*, *26*, and *27*), but its use has been justified because the rate of first electron transfer from primary to secondary quinone acceptors is roughly 10 times slower (*46*−*48*). However, recent evidence suggests that a fast component may exist in the first electron transfer (*49*, *50*). Therefore we compared P^+ reduction kinetics using Nd:YAG and xenon flashlamp actinic sources both with and without Q_B site inhibition by terbutryn (Figure 8). The 0.8-ms half-time slow phase—observed in all traces and attributed to incomplete sample reduction in the presence of 100 μM ascorbate[5]—is larger by 20% of the total P^+ amplitude for uninhibited RCs excited by the flashlamp than by the laser (Figure 8A). The different actinic sources produce identical traces for inhibited RCs (Figure 8B).

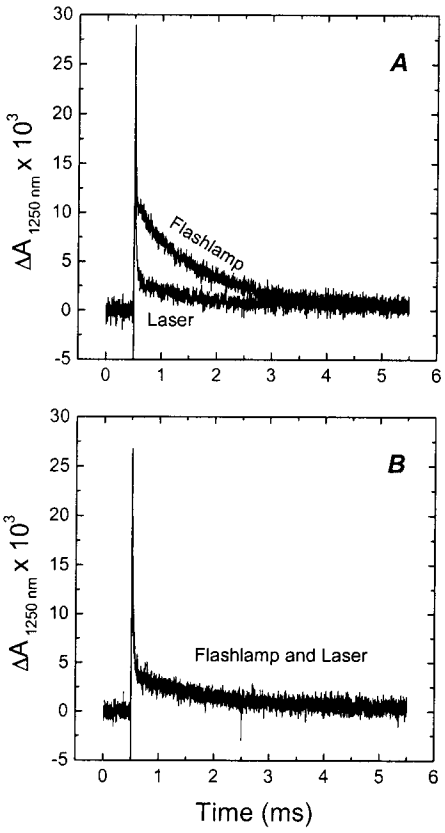

FIGURE 8: Actinic artifact of xenon flashlamps. Comparison of single flash-induced P^+ reduction kinetics by cyt *c* using xenon (flashlamp) and Nd:YAG (laser) actinic sources. (A) Conditions: 2.2 μM RCs, 10.1 μM reduced cyt *c*, 10 μM Q_6, 10 μM 1,2-naphthoquinone, 10 mM Tricine (pH 8.0), 2 mM KCl, 0.045% LDAO, and 200 μM sodium ascorbate. (B) As in panel A, except 50 μM terbutryn was added as inhibitor of the Q_B binding site. Each trace is an average of two, with 90 s dark adaptation between measurements. The traces from the two actinic sources are superimposed in panel B.

DISCUSSION

Preferential Binding. Preferential binding of both ferricytochromes *c* and c_2 to unspecified membrane component(s) has been known for many years (*34*, *51*), and preferential binding of oxidized cyt *c* to RCs reconstituted into neutral phosphatidylcholine vesicles (PC RCs) has also been demonstrated (*30*). However, this is the first report of preferential binding of oxidized cytochrome to detergent solubilized RCs. This finding establishes that preferential binding is a property inherent to RC−cyt *c* complexes and not a consequence of protein−membrane interactions. Redox titration of the cytochrome to RC electron-transfer kinetics confirms that preferential binding occurs in the electron-transfer active complex.

The preferential binding to PC RCs found by Moser and Dutton (*30*) was slightly stronger than observed here in the ground-state redox titrations (5-fold vs 3.6-fold), and the dependence of the effective cytochrome midpoint potential on PC RC concentration was inconsistent with a single cytochrome binding site. Thus, in PC RCs, protein−lipid interactions may stabilize multiple RC−cyt *c* binding modes, with uncertain relation to electron transfer. Similar cytochrome oxidation kinetics were observed for PC RCs and LDAO solubilized RCs (LDAO RCs), yet no difference was detected in cyt *c* redox titration with and without LDAO RCs (*30*). The latter is possibly a consequence of low RC concentration relative to cytochrome. In contrast, both the ground-state and kinetic redox titrations here are consistent with simple, one-site binding.

Equilibrium Binding, K_{Dr}. The P^+ reduction kinetics obeyed the simple two-state reaction model: the slow-phase amplitude extrapolated to 2 ± 1% of the total amplitude under fully reducing conditions. This is consistent with the slow phase arising from second-order collisional electron transfer to an equilibrium population of uncomplexed RCs with $K_{Dr} = 0.17 \pm 0.03$ μM. This affinity is at the high (tight) end of previously reported values for functional binding (0.2−4 μM, from refs *3*, *26*, *30*, and *52*). The higher affinity is probably attributable to our use of Tricine (zwitterionic) buffer in place of Tris (cationic) and a consequent lower ionic strength (at least 40% lower by conductivity measurements). For highest precision, binding affinity is generally measured at concentrations closer to K_D than used here. These

[4] When measured through a red filter, the discharge profile of a flash lamp is significantly longer than without a filter.

[5] The sample was not maintained under inert conditions, and ambient oxidation was observed on a 10-min time scale, as indicated by a slowly increasing amplitude of slow phase in the Nd:YAG induced traces. The increase in slow phase amplitude was reversed by addition of extra sodium ascorbate (data not shown).

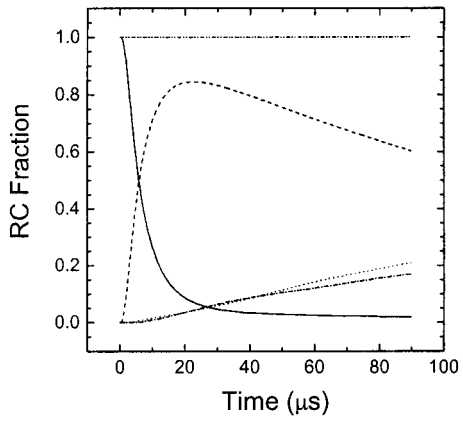

FIGURE 9: Double excitation model. Numerical solution of Scheme 1 with $c = 6$ and $k_1 = 6000\ s^{-1}$ (see text). PQ_AQ_B (solid), $PQ_A^-Q_B$ (dash), $PQ_AQ_B^-$ (dot), $P^+Q_A^-Q_B^-$ (dash dot), and total sum (dash dot dot).

kinetic experiments were designed primarily for uncovering redox-state sensitive differences in K_D, necessitating the higher concentrations of both RC and cyt *c*. Nevertheless, the magnitude of the binding we report is clearly resolved under these conditions. For instance, had K_{Dr} been a more typical value of 1 μM, approximately 10% slow-phase amplitude would have been expected instead of the 2 ± 1% observed.

Double-Hit Excitation. Some previous reports of type II cyt *c* photooxidation are likely to include double-hit artifacts from the xenon flashlamps used as actinic sources (*30*, *31*). Figure 8 demonstrates a greater amplitude of slow P^+ reduction when photoexcited by the xenon flashlamp as compared to the shorter pulse-width Nd:YAG laser. The disappearance of this effect in the presence of terbutryn is consistent with the pulse width of the flashlamp being sufficiently long to produce double-hit photoexcitation in RCs with functional secondary quinone. Terbutryn displaces ubiquinone at the Q_B site, blocking the usual electron-transfer pathway for rapid oxidation of the Q_A semiquinone formed on initial photoexcitation, and RCs with reduced Q_A are inactive for subsequent photoinduced charge separation.

Recently, question has arisen whether a fast component of first electron transfer to Q_B (k_1) exists with ubiquinone as both Q_A and Q_B (*49*, *50*). On the basis of the following scheme, a computational approach was taken to determine if the flashlamp artifact seen here is a consequence of such novel, fast first electron transfer:

Scheme 1

$$PQ_AQ_B \xrightarrow{k_l(t)} PQ_A^-Q_B \xrightarrow{k_1} PQ_AQ_B^- \xrightarrow{k_l(t)} P^+Q_A^-Q_B^-$$

where $k_l(t)$ is the time-dependent photoactivation rate proportional to the actinic light intensity with proportionality constant, *c*. The model ignores P^+ reduction by cyt *c*, assuming that the first Q_A to Q_B electron transfer is rate limiting for the second charge separation. Euler's method was used for numerical solution of Scheme 1, using the measured flashlamp discharge profile shown in Figure 7. The proportionality constant, *c*, was chosen to produce a first charge separation in 98% of RCs in the model, a typical extent of flash saturation. The solution (Figure 9) predicts at least 17% double hits with $k_1 = 6000\ s^{-1}$, a typical value for the first electron-transfer rate at pH 8.0 (*46*−*48*). This is certainly consistent with the 20% extra slow-phase amplitude observed with the flashlamp vs the laser. Contribution from significantly faster phases of Q_A to Q_B electron transfer would quickly lead to double hits greatly in excess of those observed. Therefore, the result from this simple *internal* double-flash experiment does not support the existence of a faster component of first electron transfer with native ubiquinones under the conditions employed. It is to be noted, however, that the faster components reported by Tiede et al. (*49*, *50*) are apparently sensitive to sample conditions, especially the method of quinone reconstitution. More generally, our result admonishes use of this style of flashlamp for photochemical reactions that become re-excitable at rates as slow as the consensus first electron transfer. With the flashlamp used here, reducing double turnover events to 1% would require limiting the rate of appearance of the second photoexcitable state to no more than $300\ s^{-1}$. However, this cannot be used as a general rule-of-thumb, because discharge profiles vary between flashlamps and with age as well as with spectral distribution. We have observed fwhm ranging from 8 to 25 μs with our flashlamps (EG&G, FX-200), so these results probably represent a worst case. Nevertheless, even the shortest 8-μs pulse profile produced 10% double-hits in our model.

Ferricytochrome c Dissociation. The 0.8-ms half-time slow phase of P^+ reduction observed in all traces in Figure 8 is significantly slower than previously reported for cyt *c* (*3*, *26*, *30*). Although the mechanism giving rise to slow-phase behavior is unclear in previous studies, here it is easily ascribed to deliberate, incomplete cyt *c* reduction.[5] Under low ionic strength conditions, such as used here, P^+ reduction after an initial donor side turnover event is rate limited by slow release of photooxidized cytochrome formed on the first turnover (*53*, *54*). This has been confirmed for steady-state turnover under a wide variety of conditions (*55*). Therefore, it is consistent that both the slow phase caused by the equilibrium population of RCs with bound, oxidized cytochrome and the additional slow phase caused by doubly hit RCs should have the same rate: in the presence of excess reduced cytochrome, both reactions are limited by dissociation of oxidized cytochrome.

The slower rate observed here, compared to previous work, probably reflects a lower ionic strength. Using our binding affinity for the oxidized form (0.05 μM) and a diffusion limit for the association rate constant similar to that for reduced cyt *c* of $6 \times 10^9\ M^{-1}\ s^{-1}$ (enhanced by electrostatic interaction; see refs *8* and *26*) yields an off-rate of $300\ s^{-1}$ (half-time = 2 ms). For proper comparison, however, the parameters needed are those with photooxidized reaction center (P^+). We therefore consider this to be consistent with the 0.8-ms slow phase observed here.

Moser and Dutton (*30*) also invoked a role for oxidized cyt *c* in their accounting of the cyt *c* oxidation kinetics. They proposed that oxidized cyt *c* produced *during* the flash by one RC could act as a competitive inhibitor of P^+ reduction at another RC. This would require that the dissociation of oxidized cyt *c* be very fast, which is quite distinct—and apparently incompatible—with our findings. However, the effect was only demonstrated at very low concentrations of cytochrome and in the presence of high concentrations of

glycerol, resulting in re-reduction times in the tens of milliseconds range.

Revisiting the Distal to Proximal Model for cyt c. Although simple cytochrome oxidation kinetics using cyt *c* as donor were reported in ref *27*, the literature is dominated by examples of type II cyt *c* oxidation kinetics (*3*, *26*, *30*, *31*). Overfield and Wraight (*26*) found that the half-time of total cytochrome photooxidation appeared to plateau at about 30 μs, but they clearly underestimated the equimolar RC−cytochrome concentrations necessary to saturate the binding site affinity that they also found (1−1.5 μM). They interpreted their results in the context of a model proposed earlier to account for complicated cyt c_2 oxidation kinetics (*32*), but in retrospect, these cyt *c* concentration dependencies might be consistent with the simple kinetic model. The 30 μs apparent half-time is slower than rates that others have interpreted as originating from rapid electron-transfer active complexes, but a faster (2 μs) component was also detected beneath this kinetic. This is qualitatively similar to the two fast phases (cytochrome concentration independent) demonstrated by Tiede et al. (*3*) with half-times of 16 ± 3 and 0.7 ± 0.1 μs (7:3 ratio) and by Long et al. (*14*) with half-times of 6 and 38 μs (1:1 ratio). Rosen et al. (*27*) reported a single 14 μs half-time component of electron transfer.

The slow-phase behavior in two of the remaining studies (*30*, *31*) may be an artifact of double-hits. This was certainly the case in our earlier study. We performed double-flash experiments and demonstrated that the slow-phase behavior seen in single flash traces also appears in the *difference* between single and double-flash traces (*31*). The difference between single and double-flash traces reflects cytochrome oxidation by RCs that have already undergone a complete donor side turnover. The observation that the slow phase in the difference data is independent of the time between flashes was originally interpreted as evidence of multiple cytochrome binding to the RC. However, we can now attribute the effect to an artifact of double-hits. In both cases (single and double flashes), the slow phase originates from rate-limiting dissociation of oxidized cytochrome photoproduct.

In the very extensive study by Tiede et al. (*3*), three different RC preparations exhibited type II cyt *c* oxidation kinetics. In addition to two cyt *c* concentration-independent fast phases, each RC preparation also produced a cytochrome concentration-dependent slow phase that accelerated to a pseudo-first-order limit at high cytochrome. The kinetics were activated by short pulse-width laser and monitored by absorbance changes at 860 nm. A short baseline time was used (50 ms) to prevent actinic effects from the measuring beam, the results were corroborated with measurements at other less or nonactinic wavelengths, and redox mediators were used to equilibrate the cytochrome pool to a low redox poise (100 mV). Under these conditions, and even considering tighter binding of the oxidized form, it seems unlikely that enough oxidized cytochrome could have been present to account for the 40−60% relative slow-phase amplitude seen at saturating cytochrome concentration. Consequently, we must conclude that methodological problems can explain some, but not all, examples of complicated RC−cyt *c* electron-transfer kinetics.

REFERENCES

1. Gunner, M. R. (1991) *Curr. Top. Bioenerg. 16*, 319−367.
2. Shinkarev, V. P., and Wraight, C. A. (1993) *The Photosynthetic Reaction Center, Vol. I* (Norris, J. R., and Deisenhofer, J., Eds.) pp 193−255, Academic Press, New York.
3. Tiede, D. M., Vashishta, A., and Gunner, M. R. (1993) *Biochemistry 32*, 4515−4531.
4. Tiede, D. M., and Dutton, P. L. (1993) *The Photosynthetic Reaction Center, Vol. I* (Norris, J. R., and Deisenhofer, J., Eds.) pp 257−288, Academic Press, New York.
5. Mathis, P. (1994) *Biochim. Biophys. Acta 1187*, 177−180.
6. Prince, R. C., Cogdell, R. J., and Crofts, A. R. (1974) *Biochim. Biophys. Acta 347*, 1−13.
7. Ke, B., Chaney, T. H., and Reed, D. W. (1970) *Biochim. Biophys. Acta 216*, 373−383.
8. Overfield, R. E., and Wraight, C. A. (1980) *Biochemistry 19*, 3322−3327.
9. Allen, J. P., Feher, G., Yeates, T. O., Komiya, H., and Rees, D. C. (1987) *Proc. Natl. Acad. Sci. U.S.A. 84*, 6162−6166.
10. Tiede, D. M., and Chang, C.-H. (1988) *Isr. J. Chem. 28*, 183−191.
11. Hall, J., Ayres, M., Zha, X., O'Brien, P., Durham, B., Knaff, D., and Millett, F. (1987) *J. Biol. Chem. 262*, 11046−11051.
12. Tiede, D. M. (1987) *Biochemistry 26*, 397−410.
13. Van der Wal, H. N., Van Grondelle, R., Millett, F., and Knaff, D. B. (1987) *Biochim. Biophys. Acta 893*, 490−498.
14. Long, J. E., Durham, B., Okamura, M., and Millett, F. (1989) *Biochemistry 28*, 6970−6974.
15. Tiede, D. M., and Vashishta, A. (1991) *Mol. Cryst. Liq. Cryst. 194*, 191−200.
16. Caffrey, M. S., Bartsch, R. G., and Cusanovich, M. A. (1992) *J. Biol. Chem. 267*, 6317−6321.
17. Margoliash, E., and Bosshard, H. R. (1983) *Trends Biochem. Sci. 8*, 316−320.
18. Adir, N., Axelrod, H. L., Beroza, P., Isaacson, R. A., Rongey, S. H., Okamura, M. Y., and Feher, G. (1996) *Biochemistry 35*, 2535−2547.
19. Chang, C.-H., Tiede, D., Tang, J., Smith, U., Norris, J., and Schiffer, M. (1986) *FEBS Lett. 205*, 82−86.
20. Allen, J. P., Feher, G., Yeates, T. O., Komiya, H., and Rees, D. C. (1988) *Proc. Natl. Acad. Sci. U.S.A. 85*, 8487−8491.
21. Ermler, U., Michel, H., and Schiffer, M. (1994) *J. Bioenerg. Biomembr. 26*, 5−15.
22. Arnoux, B., Gaucher, J. F., Ducruix, A., and Reiss-Husson, F. (1995) *Acta Crystallogr. D51*, 368−379.
23. Stowell, M. H. B., Mcphillips, T. M., Rees, D. C., Soltis, S. M., Abresch, E., and Feher, G. (1997) *Science 276*, 812−816.
24. Bushnell, G. W., Louie, G. V., and Brayer, G. D. (1990) *J. Mol. Biol. 214*, 585−595.
25. Axelrod, H. L., and Feher, G. (1994) *Acta Crystallogr. D50*, 596−602.
26. Overfield, R. E., and Wraight, C. A. (1986) *Photosyn. Res. 9*, 167−179.
27. Rosen, D., Okamura, M. Y., Abresch, E. C., Valkirs, G. E., and Feher, G. (1983) *Biochemistry 22*, 335−341.
28. Venturoli, G., Mallardi, A., and Mathis, P. (1993) *Biochemistry 32*, 13245−13253.
29. Wang, S., Li, X., Williams, J. C., Allen, J. P., and Mathis, P. (1994) *Biochemistry 33*, 8306−8312.
30. Moser, C. C., and Dutton, P. L. (1988) *Biochemistry 27*, 2450−2461.
31. Larson, J. W., and Wraight, C. A. (2000) *Biophys. J. 78*, 339A.
32. Overfield, R. E., Wraight, C. A., and DeVault, D. (1979) *FEBS Lett. 105*, 137−142.
33. Wachtveitl, J., Farchaus, J. W., Mathis, P., and Oesterhelt, D. (1993) *Biochemistry 32*, 10894−10904.
34. Dutton, P. L., Petty, K. M., Bonner, H. S., and Morse, S. D. (1975) *Biochim. Biophys. Acta 387*, 536−556.
35. Tiede, D. M., Littrell, K., Marone, P. A., Zhang, R., and Thiyagarajan, P. (2000) *J. Appl. Crystallogr. 33*, 560−564.
36. Speck, S. H., and Margoliash, E. (1984) *J. Biol. Chem. 259*, 1064−1072.
37. Vanderkooi, J., and Erecinska, M. (1974) *Arch. Biochem. Biophys. 162*, 385−391.
38. Maróti, P., and Wraight, C. A. (1988) *Biochim. Biophys. Acta 934*, 329−347.

39. Feher, G., and Okamura, M. Y. (1978) *The Photosynthetic Bacteria* (Clayton, R. K., and Sistrom, W. R., Eds.) pp 349−386, Plenum Press, New York.
40. Straley, S. C., Parson, W. W., Mauzerall, D. C., and Clayton, R. K. (1973) *Biochim. Biophys. Acta 305*, 597−609.
41. Margoliash, E., and Frohwirt, N. (1959) *Biochem. J. 71*, 570−572.
42. O'Reilly, J. E. (1973) *Biochim. Biophys. Acta 292*, 509−515.
43. Braun, M. (1993) *Differential Equations and Their Applications: An Introduction to Applied Mathematics*, 4th ed., pp 100−106, Springer−Verlag, New York.
44. Henderson, R. W., and Rawlinson, W. A. (1956) *Biochem. J. 62*, 21.
45. Drepper, F., Hippler, M., Nitschke, W., and Haehnel, W. (1996) *Biochemistry 35*, 1282−1295.
46. Verméglio, A., and Clayton, R. K. (1977) *Biochim. Biophys. Acta 461*, 159−165.
47. Wraight, C. A. (1979) *Biochim. Biophys. Acta 548*, 309−327.
48. Kleinfeld, D., Okamura, M. Y., and Feher, G. (1984) *Biochim. Biophys. Acta 766*, 126−140.
49. Tiede, D. M., Vazquez, J., Cordova, J., and Marone, P. A. (1996) *Biochemistry 35*, 10763−10775.
50. Tiede, D. M., Utschig, L., Hanson, D. K., and Gallo, D. M. (1998) *Photosynth. Res. 55*, 267−273.
51. Dutton, P. L., Wilson, D. F., and Lee, C. P. (1970) *Biochemistry 9*, 5077−5082.
52. Yang, Q., Liu, X. Y., Hara, M., Lundahl, P., and Miyake, J. (2000) *Anal. Biochem. 280* (1), 94−102.
53. Larson, J. W., and Wraight, C. A. (1998) *Biophys. J. 74*, A76.
54. Larson, J. W., Wells, T. A., and Wraight, C. A. (1999) *Biophys. J. 76*, A239.
55. Gerencsér, L., Laczkó, G., and Maróti, P. (1999) *Biochemistry 38*, 16866−16875.

BI0012991